Mathematical Geology, Vol. 35, No. 3, April 2003 (© 2003)

Modelling Compositional Change: The Example of Chemical Weathering of Granitoid Rocks[1]

Hilmar von Eynatten,[2,3] Carles Barceló-Vidal,[4] and Vera Pawlowsky-Glahn[4]

Perturbation on the simplex is an operation which can be used to numerically describe changes in the composition of, for example, soils, sediments, or rocks. The combination of perturbation and power transformation provides a strong tool for analyzing compositional linear processes in the simplex. When the process is constrained in the sense of a well-known starting (or final) composition, non-centred principal component analysis can be used to estimate the leading perturbation vector of the process. Applying these mathematical tools to chemical major element data from a weathering profile developed on granitoid rocks allows us to model the compositional changes associated with the process of chemical weathering. The comparison of these results with the compositional linear trend defined by erosional products of several of the world's major drainage systems yields close similarities. The latter observation allows for a mathematical formulation of a global mean weathering trend within the system Al_2O_3–CaO–Na_2O–K_2O. We further demonstrate the usefulness of the approach for validating processes behind individual trends and for combining the effects of different processes which modify the composition of soils, sediments, and rocks. Alternatives to the Chemical Index of Alteration (CIA) are discussed to obtain a translation-invariant scale for the process of chemical weathering.

KEY WORDS: Aitchison geometry, perturbation, power transformation, compositional linear trend, chemical weathering, Chemical Index of Alteration.

INTRODUCTION

Chemical weathering refers to chemical and mineralogical transformations induced by the interaction of rainwater and rocks at the earth's surface in the soil zone. It plays a major role in the global hydrogeochemical cycle and is among the most important processes determining the composition of sediments (Leeder, 1999). Chemical weathering reactions are mainly transformations of feldspars

[1]Received 5 March 2002; accepted 14 February 2003.

[2]Institut für Geowissenschaften, FSU Jena, Burgweg 11, D-07743 Jena, Germany.

[3]Present address: Department of Sedimentology and Environmental Geology, Geoscience Centre, University of Göttingen, Goldschmidtstrasse 3, D-37077 Göttingen, Germany; e-mail: hilmar.von.eynatten@geo.uni-goetttingen.de.

[4]Departament d'Informàtica i Matemàtica Aplicada, Universitat de Girona, Campus Montilivi – P4, E-17071 Girona, Spain.

(albite, anorthite, K-feldspar), primary phyllosilicates (muscovite, biotite), mafic minerals (amphibole, pyroxene), and volcanic glass into secondary phyllosilicates like illite, smectite, and kaolinite, and Al-hydroxides like gibbsite. Among these reactions, the transformation of feldspar to phyllosilicates is the most important because feldspar constitutes about 50–60% of the earth's upper crust (Nesbitt and Young, 1984). The overall reaction involving, for example, albite and kaolinite is

$$\underset{}{2H_2CO_3} + \underset{\text{(Albite)}}{2NaAlSi_3O_8} + H_2O \rightarrow \underset{\text{(Kaolinite)}}{Al_2Si_2O_5(OH)_4} + 2Na^+ + 2HCO_3^- + 4SiO_2(aq.)$$

Analogous reactions can be obtained by substituting other primary Al-silicates such as K-feldspar for albite and other clay minerals such as illite for kaolinite. For these reactions under natural conditions Al is generally considered to be insoluble and remains in solid phases whereas alkalis and alkaline earths (mostly Na, K, Ca, Mg) and silica increase in weathering solutions as being removed from the solid phases (Nesbitt and Young, 1984). Thus, progressive chemical weathering of rocks exposed to the earth's surface can be described as a continuous change of the chemical composition of the material in the weathering zone.

Chemical compositions are by definition vectors of which each component is nonnegative and with all components summing to a constant c (usually 1 or 100%). As stated by Aitchison (1986), the sample space for such D-part compositional data is not the D-dimensional real space $\Re^D$ but the simplex. We denote the sample space by S^D to emphasize that vectors with D parts or components represent its elements, following standard practice in the geosciences, as for example in the classical ternary diagrams. S^D can be viewed as a subset of the standard simplex, Δ, which is a convex subset of $\Re^D$ (Schechter, 1997), and as a $(D-1)$-dimensional vector space with scalar field $\Re$ in itself. This fact represents a powerful mathematical tool for the development of new modelling techniques and is the basis of the approach here presented.

Special techniques are necessary to analyze compositional data within this approach with statistical rigour. In this contribution an attempt is made to model the compositional changes caused by progressive chemical weathering using mathematical operations in the simplex like perturbation, power transformation, and noncentred principal component analysis which take into account the specific nature of compositional data. The modelling approach introduced here can be applied to a wide range of processes and combinations of processes causing compositional changes. The case study used is a well-known and often-cited example from a weathering profile developed on the Toorongo granodiorite in South Australia (Nesbitt and Markovics, 1997; Nesbitt, Markovics, and Price, 1980). The results obtained for this weathering profile are compared with other case studies and the potential of the approach for validating the process behind individual trends and

for combining the effects of different processes modifying the composition of soils and sediments are commented on.

CASE STUDY

The Toorongo weathering profile is developed on a Palaeozoic granodiorite exposed in the highlands of eastern Victoria about 100 km east of Melbourne (South Australia). Climate is moderate with average temperatures ranging from 0–50°C in winter to 25–30°C in summer. Annual precipitation rates are approximately 1500 mm (Nesbitt and Markovics, 1997). The initial (unweathered) composition of the granodiorite is similar to average upper continental crust implying that this example is suitable for deriving some general characteristics of the chemical weathering of the continental crust. The sampled weathering profile includes four zones which are ordered from almost no alteration to very strong alteration (Nesbitt and Markovics, 1997): (1) the corestone zone (samples 1 and 2), (2) the exfoliate zone (competent layers of granodiorite separated by ellipsoidal fractures from the corestone, samples 3–7), (3) the textured clay zone (incompetent layers composed mostly of quartz and clay minerals but still showing granitoid texture, samples 8–13), and (4) the massive fracture fill (texturally massive fine-grained clay, samples 14 and 15).

The major element data from the 15 samples are listed in Table 1. The data comprise 12 variables including both ferrous and ferric iron oxide and water. Total iron is calculated by $FeO(t) = FeO + 0.90Fe_2O_3$. The Chemical Index of Alteration (CIA) is calculated by $CIA = 100Al_2O_3/(Al_2O_3 + CaO^* + Na_2O + K_2O)$ by using molar percentages of the major element oxides. Nesbitt and Young (1982) have defined this index, which is now widely used in the geosciences, to describe the degree of chemical weathering of a sample. CaO^* is restricted to CaO associated with the silicate phases which means that there must be corrections for CaO associated with phosphate phases (e.g. apatite) or carbonate phases. If no Ca-carbonate is present (as in this case study), the correction for phosphate phases is straightforward by $CaO^* = CaO - 3.33P_2O_5$ assuming that all P_2O_5 is associated with apatite. If Ca-carbonate is present, corrections are either more complicated or simple assumptions have to be made (e.g., McLennan, 1993). Fresh granitoid rocks usually have CIA values ranging from 45 to 55 whereas secondary minerals constituting the weathered material have CIA values ranging from around 80 (e.g., illite) to 100 (e.g., kaolinite). Thus a complete weathering profile developed on granitoid rocks should start with CIA values around 50 and end up with CIA values close to 100 (Table 1). Figure 1 illustrates this trend for the selected sample suite in the A-CN-K ternary diagram.

The overall compositional variability of the samples from the Toorongo weathering profile is demonstrated using biplots of the whole data set with all variables (Fig. 2(A)) and with all variables except for H_2O and with FeO and Fe_2O_3 substituted by total iron FeO(t) (Fig. 2(B)). The latter is chosen for practical

Table 1. Chemical Data From the Toorongo Weathering Profile in wt% and mol% (Nesbitt and Markovics, 1997)

No.	SiO_2	TiO_2	Al_2O_3	Fe_2O_3	FeO	MnO	MgO	CaO	Na_2O	K_20	P_2O_5	H_2O	FeO(t)	CIA
1	64.26 (1.0694)	0.88 (0.0110)	15.67 (0.1537)	0.67 (0.0042)	4.43 (0.0617)	0.09 (0.0013)	2.63 (0.0653)	4.31 (0.0769)	3.44 (0.0555)	2.58 (0.0274)	0.26 (0.0018)	1.05 (0.0583)	5.03 (0.0700)	**50.01**
2	64.34 (1.0707)	0.89 (0.0111)	15.59 (0.1529)	0.74 (0.0046)	4.34 (0.0604)	0.09 (0.0013)	2.64 (0.0655)	4.27 (0.0761)	3.41 (0.0550)	2.63 (0.0279)	0.28 (0.0020)	1.13 (0.0627)	5.01 (0.0697)	**50.06**
3	64.22 (1.0687)	0.88 (0.0110)	15.65 (0.1535)	0.87 (0.0054)	4.13 (0.0575)	0.09 (0.0013)	2.52 (0.0625)	3.99 (0.0711)	3.33 (0.0537)	2.53 (0.0269)	0.24 (0.0017)	1.73 (0.0960)	4.91 (0.0684)	**51.23**
4	64.27 (1.0696)	0.91 (0.0114)	15.68 (0.1538)	0.94 (0.0059)	4.23 (0.0589)	0.09 (0.0013)	2.63 (0.0653)	3.94 (0.0703)	3.26 (0.0526)	2.52 (0.0268)	0.23 (0.0016)	1.51 (0.0838)	5.08 (0.0706)	**51.61**
5	64.33 (1.0706)	0.88 (0.0110)	15.45 (0.1515)	0.79 (0.0049)	4.23 (0.0589)	0.09 (0.0013)	2.63 (0.0653)	3.70 (0.0660)	3.28 (0.0529)	2.46 (0.0261)	0.25 (0.0018)	2.03 (0.1127)	4.94 (0.0688)	**52.13**
6	64.01 (1.0652)	0.87 (0.0109)	15.80 (0.1550)	1.24 (0.0078)	3.96 (0.0551)	0.09 (0.0013)	2.62 (0.0650)	3.72 (0.0663)	3.32 (0.0536)	2.63 (0.0279)	0.26 (0.0018)	2.09 (0.1160)	5.08 (0.0706)	**52.23**
7	63.43 (1.0556)	0.86 (0.0108)	15.51 (0.1521)	1.15 (0.0072)	3.84 (0.0534)	0.09 (0.0013)	2.59 (0.0643)	3.30 (0.0588)	3.11 (0.0502)	2.65 (0.0281)	0.25 (0.0018)	2.48 (0.1377)	4.88 (0.0678)	**53.67**
8	61.08 (1.0165)	0.80 (0.0100)	17.71 (0.1737)	2.41 (0.0151)	2.48 (0.0345)	0.08 (0.0011)	2.31 (0.0573)	2.15 (0.0383)	2.09 (0.0337)	2.10 (0.0223)	0.20 (0.0014)	6.22 (0.3453)	4.65 (0.0647)	**65.95**
9	57.98 (0.9649)	0.79 (0.0099)	19.76 (0.1938)	3.12 (0.0195)	1.65 (0.0230)	0.07 (0.0010)	2.22 (0.0551)	1.33 (0.0237)	1.85 (0.0298)	2.23 (0.0237)	0.19 (0.0013)	9.06 (0.5029)	4.46 (0.0620)	**72.70**
10	59.56 (0.9912)	0.81 (0.0101)	18.24 (0.1789)	3.70 (0.0232)	1.36 (0.0189)	0.07 (0.0010)	2.21 (0.0548)	1.06 (0.0189)	1.25 (0.0202)	2.40 (0.0255)	0.18 (0.0013)	8.60 (0.4774)	4.69 (0.0653)	**74.78**
11	60.03 (0.9990)	0.79 (0.0099)	18.36 (0.1801)	3.80 (0.0238)	1.04 (0.0145)	0.06 (0.0008)	2.10 (0.0521)	0.60 (0.0107)	0.47 (0.0076)	2.48 (0.0263)	0.17 (0.0012)	8.80 (0.4885)	4.46 (0.0621)	**81.59**
12	57.58 (0.9582)	0.78 (0.0098)	20.03 (0.1964)	3.77 (0.0236)	1.08 (0.0150)	0.06 (0.0008)	2.07 (0.0514)	0.54 (0.0096)	0.43 (0.0069)	2.44 (0.0259)	0.16 (0.0011)	10.10 (0.5606)	4.47 (0.0623)	**83.54**
13	59.30 (0.9869)	0.74 (0.0093)	19.21 (0.1884)	3.87 (0.0242)	0.79 (0.0110)	0.05 (0.0007)	1.88 (0.0467)	0.34 (0.0061)	0.25 (0.0040)	2.28 (0.0242)	0.16 (0.0011)	11.03 (0.6123)	4.27 (0.0595)	**86.05**
14	49.56 (0.8248)	0.44 (0.0055)	28.20 (0.2766)	2.57 (0.0161)	0.22 (0.0031)	0.09 (0.0013)	1.01 (0.0251)	0.07 (0.0012)	0.09 (0.0015)	1.53 (0.0162)	0.13 (0.0009)	15.28 (0.8482)	2.53 (0.0353)	**93.99**
15	53.13 (0.8842)	0.41 (0.0051)	29.99 (0.2941)	2.11 (0.0132)	0.13 (0.0018)	0.02 (0.0003)	0.86 (0.0213)	0.03 (0.0005)	0.07 (0.0011)	1.30 (0.0138)	0.11 (0.0008)	11.92 (0.6617)	2.03 (0.0282)	**95.17**

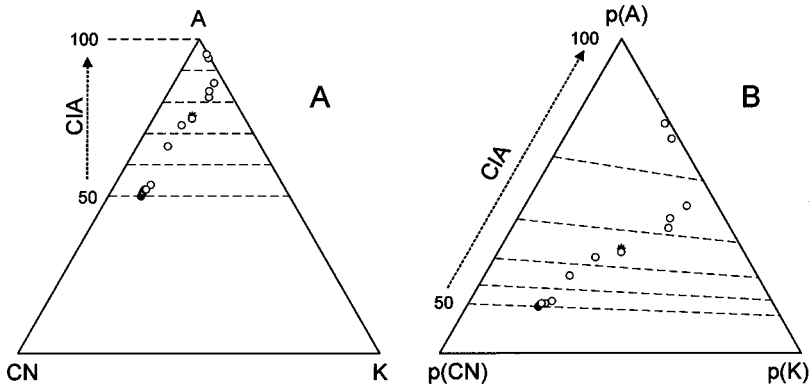

Figure 1. Samples of the Toorongo weathering profile plotted in the A-CN-K diagram with A = Al_2O_3, CN = CaO^*+ Na_2O, and K = K_2O, all in molar percentages (Nesbitt and Markovics, 1997; for data, see Table 1). Stars indicate geometric mean of the sample suite. Filled circles are the geometric average of samples 1 and 2 from the corestone zone of the weathering profile and are considered an approximation for the initial composition of the granodiorite. Grid with CIA values from 50 to 100 is also shown. (A): Normal diagram, (B): centred diagram obtained by perturbation of data and grid with the inverse of the geometric mean of the data set (see von Eynatten, Pawlowsky-Glahn, and Egozcue, 2002, for details).

reasons because chemical data sets (especially XRF-data) often do not separate between ferric and ferrous iron and water content is not precisely measured. Biplots describe graphically the pattern of relative variation of a multivariate data set by projection onto a plane fixed by the first and second principal components. A principal advantage of biplots is that both samples and variables are represented (for details of biplot techniques and interpretations in general, see Gabriel, 1971; for biplots for compositional data, see Aitchison, 1990; Aitchison and Greenacre, 2002; von Eynatten, Barceló-Vidal, and Pawlowsky-Glahn, 2003). The two biplots indicate that the data set follows essentially a one-dimensional pattern with >90% of the total variability explained by the first principal component (93.5 and 95.6%, respectively, Fig. 2). The first principal component orders the samples in exactly the serial listing of Table 1 with the exception of samples 3 and 4 being exchanged in the first biplot (Fig. 2(A)). Thus, the overall ranking of samples with respect to the degree of chemical weathering obtained by CIA is similar to the ranking obtained by the first principal component. No external variable (e.g., grain size, distance from corestone) for the ordering of samples independent from composition is available for this case study.

METHODOLOGICAL APPROACH

The operations of perturbation and power transformation in the simplex S^D and their properties have been first given in Aitchison (1986). A theoretical

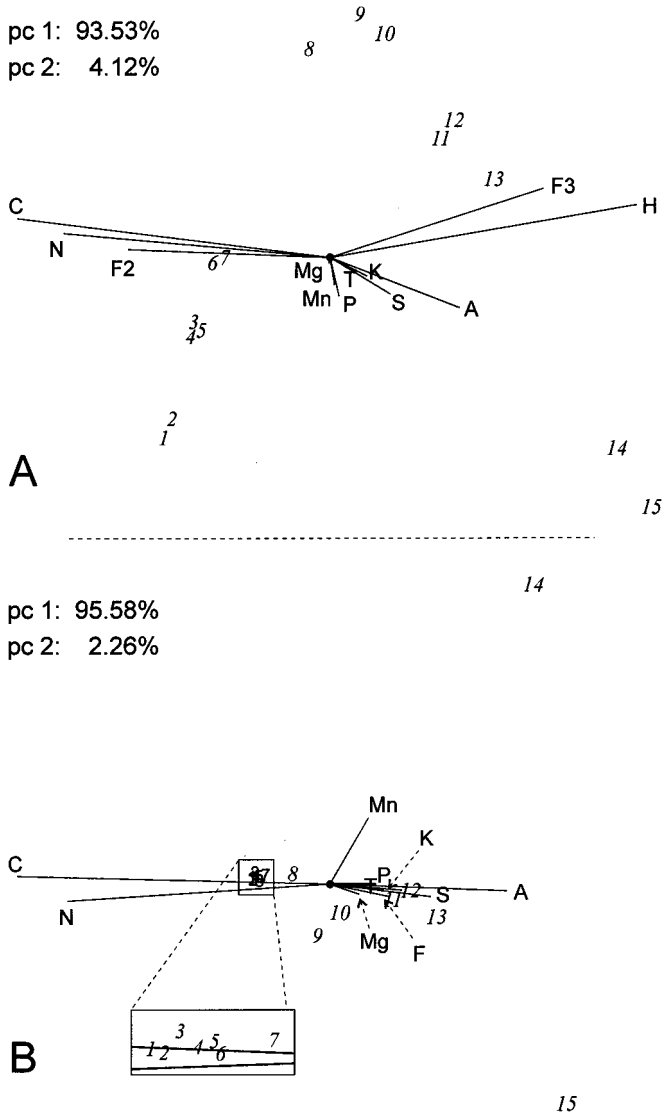

Figure 2. Biplots of samples 1–15 (Table 1) with all variables ((A), S^{12}) and all variables except for H_2O and with total iron expressed as FeO(t) ((B), S^{10}). Percentages indicate proportion of total variability explained by first and second principal components (pc). The centre of biplots (filled circle) represents the geometric mean of the data set, x-axis is first, and y-axis is second principal component. A = Al_2O_3, C = CaO, F2 = FeO, F3 = Fe_2O_3, F = FeO(t), H = H_2O, K = K_2O, Mg = MgO, Mn = MnO, N = Na_2O, P = P_2O_5, S = SiO_2, and T = TiO_2.

foundation can be found in Barceló-Vidal, Martín-Fernández, and Pawlowsky-Glahn (2001), a proof of the vector space structure in Pawlowsky-Glahn and Egozcue (2002), and a practical illustration in von Eynatten, Pawlowsky-Glahn, and Egozcue (2002). For the purpose of this paper, we recall these two operations:

(i) *perturbing* a composition $\mathbf{x} = [x_1, \ldots, x_D]$ in S^D by a composition $\mathbf{p} = [p_1, \ldots, p_D]$ in S^D results in a new composition $\mathbf{y} = \mathbf{p} \oplus \mathbf{x} = C[p_1x_1, \ldots, p_Dx_D]$ in S^D, where C denotes the closure operator, i.e., each component of the vector is divided by the sum of all its components and multiplied by a constant c (usually 1 or 100%) depending on how the components have been measured; and

(ii) the *power transformation* of a composition $\mathbf{x} = [x_1, \ldots, x_D]$ in S^D by a real constant or scalar $k \in \Re$ results in a new composition $\mathbf{y} = k \otimes \mathbf{x} = C[{x_1}^k, \ldots, {x_D}^k]$ in S^D.

These two operations give the simplex S^D a $(D-1)$-dimensional vector space structure. The neutral element is the composition $\mathbf{e} = C[1, \ldots, 1] = [1/D, \ldots 1/D]$ and the inverse $\mathbf{x}^{-1}$ of a composition $\mathbf{x} = [x_1, \ldots, x_D]$ is given by the composition $C[1/x_1, \ldots, 1/x_D]$. The *centered logratio transformation* clr from S^D to $\Re^D$, given by $\text{clr}\,\mathbf{x} = [\log(x_1/g(\mathbf{x})), \ldots, \log(x_D/g(\mathbf{x}))]$, for each $\mathbf{x}$ in S^D, where g(**x**) is the geometric mean of the components of the composition **x**, allows the definition of a compositional inner product $\langle\,,\,\rangle_a$ in S^D by $\langle \mathbf{x}, \mathbf{y}\rangle_a = \langle \text{clr}\mathbf{x}, \text{clr}\mathbf{y}\rangle$, for each **x**, **y** in S^D, where $\langle\,,\,\rangle$ stands for the common inner product in $\Re^D$. In this manner the simplex S^D becomes a linear vector space. To avoid confusion with the usual Euclidean geometry in real spaces, we call the geometry in the simplex, induced by the vector space structure and the inner product given above, *Aitchison geometry*, and use an *a* as subindex to distinguish operations within the simplex from operations in real space, whenever necessary. The compositional length of a composition **x** in S^D will be given by $|\,\mathbf{x}\,|_a = \langle \text{clr}\mathbf{x}, \text{clr}\mathbf{x}\rangle^{1/2}$.

Perturbation and power transformations can be combined to define compositional lines in S^D, lines that allow us to describe trends of compositional observations. We call those trends *compositional linear trends*. Any compositional linear trend is determined by an initial composition **a** and a unitary composition **p** which defines the direction of the trend. Then, any composition **y** on the linear trend is perfectly determined by a scalar *k* such that

$$\mathbf{y} = \mathbf{a} \oplus (k \otimes \mathbf{p}) = C[a_1 {p_1}^k, \ldots, a_D {p_D}^k]. \tag{1}$$

We will symbolize by $L_a(\mathbf{a}; \mathbf{p})$ the compositional linear trend determined by the initial composition **a** and with direction given by the unitary composition **p**. We will also symbolize either by $\mathbf{y}(k)$ or by $\mathbf{y}_k$ the composition given by (1). From (1)

it is easy to prove an important property which is characteristic of compositional linear trends:

$$\frac{d \log\left(\frac{y_j(k)}{y_r(k)}\right)}{dk} = \log\left(\frac{p_j}{p_r}\right), \text{ for each } k \in \Re \text{ and for each } j, r = 1, \ldots, D.$$

That is to say, the logarithmic derivative with respect to k of any ratio $y_j(k)/y_r(k)$ is constant and equal to $\log(p_j/p_r)$ along the trend. Therefore, if $p_j = p_r$, the ratio $y_j(k)/y_r(k)$ will be constant along the trend. Similarly, if $p_j > p_r$ [$p_j < p_r$] the ratio $y_j(k)/y_r(k)$ will increase (decrease) along the trend when k increases. Figure 3 illustrates a linear trend $L_a(\mathbf{a}; \mathbf{p})$ in S^3, with $\mathbf{a} = [0.20, 0.65, 0.15]$ and $\mathbf{p} = [0.53, 0.13, 0.34]$.

Adjusting a linear trend with known starting point $\mathbf{a}$ to a set of observations $\mathbf{x}_1, \ldots, \mathbf{x}_n$ in S^D consists in finding an axis going through $\mathbf{a}$ which explains as much as possible of the total simplicial variability $\sum | \mathbf{x}_i \oplus \mathbf{a}^{-1}|_a{}^2$ of $\mathbf{x}_1, \ldots, \mathbf{x}_n$ with respect to $\mathbf{a}$. This problem is well known in noncentral principal component analysis (see Lebart, Morineau, and Piron, 1995, Ch. 1, for a detailed theoretical development). Noncentral PCA finds the unitary eigenvectors $\mathbf{v}_1, \ldots, \mathbf{v}_D$ and corresponding eigenvalues $\lambda_1, \ldots, \lambda_D$ of the $D \times D$ product matrix $\mathbf{Z}'\mathbf{Z}$, where $\mathbf{Z}$ is the $n \times D$ matrix whose n rows are the vectors $\text{clr}\, \mathbf{x}_1 - \text{clr}\, \mathbf{a}, \ldots, \text{clr}\, \mathbf{x}_n - \text{clr}\, \mathbf{a}$, and the prime stands for transpose. If the eigenvalues are assumed to be in decreasing order of magnitude, $\lambda_1 \geq \ldots \geq \lambda_D$, then the vectors $\mathbf{e}_1 = \text{clr}^{-1}\mathbf{v}_1, \ldots, \mathbf{e}_{D-1} = \text{clr}^{-1}\mathbf{v}_{D-1}$ constitute an ordered orthonormal basis of the vector space S^D (the last eigenvector $\mathbf{v}_D$ is always equal to $(1/\sqrt{D})\mathbf{1}$ with eigenvalue $\lambda_D = 0$, where $\mathbf{1}$ symbolizes the vector of units in $\Re^D$) in the sense that they explain the variability of $\mathbf{x}_1, \ldots, \mathbf{x}_n$ with respect to $\mathbf{a}$ in decreasing order. In fact, the variability explained by the axis defined by $\mathbf{e}_j$ equals λ_j, for $j = 1, \ldots, D-1$, and the total variability of $\mathbf{x}_1, \ldots, \mathbf{x}_n$ with respect to $\mathbf{a}$ is given by the sum $\lambda_1 + \cdots + \lambda_{D-1}$. The resulting decomposition of the total simplicial variability is optimal in the sense of least squares in the context of the Aitchison geometry in the simplex.

Therefore, the linear trend with known starting point $\mathbf{a}$ which better adjusts the set of compositional observations $\mathbf{x}_1, \ldots, \mathbf{x}_n$ will be

$$L_a(\mathbf{a}; \text{clr}^{-1}\mathbf{v}_1). \tag{2}$$

The proportion of the total variability of $\mathbf{x}_1, \ldots, \mathbf{x}_n$ with respect to $\mathbf{a}$ retained by this trend will be given by the quotient $\lambda_1/(\lambda_1 + \ldots + \lambda_{D-1})$. This proportion allows us to judge the goodness of fit of (2) to $\mathbf{x}_1, \ldots, \mathbf{x}_n$. The orthogonal projection of a compositional observation $\mathbf{x}_i$ onto the linear trend (2) will be given by the composition $\mathbf{y}(k_i) = \mathbf{a} \oplus (k_i \otimes \mathbf{p})$, where $k_i = \langle \mathbf{x}_i \oplus \mathbf{a}^{-1}, \mathbf{p} \rangle_a$. The real number k_i indicates "how many times" the initial composition $\mathbf{a}$ has to be perturbed by $\mathbf{p}$ to

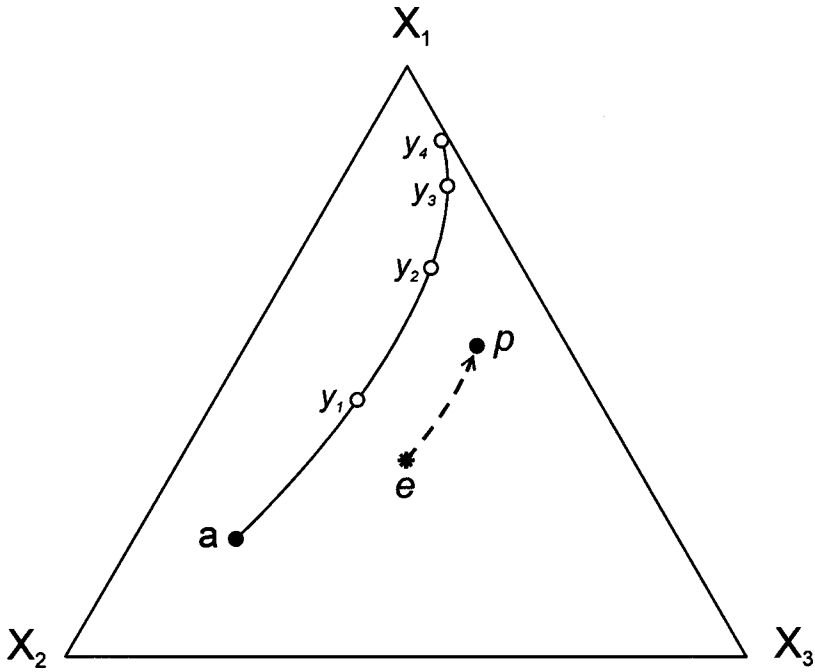

Figure 3. Vector space S^3 illustrating the properties of perturbation and power transformation. **e** is the baricentre (neutral element) of S^3, **p** denotes the perturbation vector, **a** the initial composition, and $\mathbf{y}_k = \mathbf{a} \oplus (k \otimes \mathbf{p})$ are compositions along the compositional linear trend for $k = 1, \ldots, 4$.

arrive at $\mathbf{y}(k_i)$. Therefore, if the linear trend (2) can be considered to reflect a representative process explaining the compositions $\mathbf{x}_1, \ldots, \mathbf{x}_n$, the value k_i provides a measure for the "amount" or "intensity" of the process between **a** and $\mathbf{x}_i$. In this case, the parameter k is a *translation invariant* measure, in the sense that the difference of the "intensity" of the process between $\mathbf{y}(k)$ and $\mathbf{y}(k + \Delta k)$ depends only on Δk and not on the particular value of k. In Figure 3, for example, the amount of the process leading from **a** to $\mathbf{y}_1$ equals the amount which leads from $\mathbf{y}_3$ to $\mathbf{y}_4$ because $\Delta k = 1$ in both cases. This translation invariant property of the scale k used to parameterize a process is not satisfied when using, for example, CIA values as a measure of the process (see Discussion).

In the case of the Toorongo weathering profile the starting point **a** of the weathering process is quite precisely known (the composition of the granodiorite in the almost unweathered corestone zone). But, in other processes observed, the starting point may not be identified so precisely or may be not known at all. In such cases, we suggest to calculate the standard compositional first principal component associated with the compositions $\mathbf{x}_1, \ldots, \mathbf{x}_n$, and to use as a reasonable

approximation to the starting point **a** of the compositional linear trend the orthogonal projection of the first composition $\mathbf{x}_1$ of the process onto the first principal component.

RESULTS

The biplots in Figure 2 already suggest that the process of chemical weathering as defined by the Toorongo weathering profile is essentially one-dimensional and dominated by the variables CaO, H_2O, Na_2O, Fe_2O_3, FeO, and Al_2O_3 in descending order with respect to their influence on the first principal component.

To evaluate the relative variations of all variables of the data set, we have adjusted a compositional linear trend $L_a(\mathbf{a}; \mathbf{p})$ using as initial composition **a** the geometric mean $0.5 \otimes (\mathbf{x}_1 \oplus \mathbf{x}_2)$ of the first two compositions $\mathbf{x}_1$ and $\mathbf{x}_2$ of the data set because both samples are derived from the almost unweathered corestone zone of the weathering profile. Then, the unitary perturbation **p** of the compositional linear trend $L_a(\mathbf{a}; \mathbf{p})$ has been estimated as described before from compositions $\mathbf{x}_3, \ldots, \mathbf{x}_{15}$ (Table 2). The proportion of the total variability of $\mathbf{x}_3, \ldots, \mathbf{x}_{15}$ with respect to **a** captured by this compositional linear trend is 95.9%.

For a better interpretation of relative changes, we prefer to use a rescaled version of $k \otimes \mathbf{p}$, an idea induced by the concept of *direct perturbation* suggested by Buxeda i Garrigós (1999). This rescaling does not imply any change in the model from a mathematical point of view and can be done using any scalar function $f(k)$ of k, as it holds that $k \otimes \mathbf{p} = f(k)\mathbf{1} \oplus (\mathbf{k} \otimes \mathbf{p})$, where $f(k)\mathbf{1} = f(k)[1, \ldots, 1] = [f(k), \ldots, f(k)]$ in $\Re^D$. Rescaling consists in representing $f(k)\mathbf{1} \oplus k \otimes \mathbf{p})$, before closure. In particular, one can use the inverse of any of the parts, $f(k) = p_i^{-k}$, thus obtaining a stable reference for changes in the other parts. We have chosen Al_2O_3 as denominator because Al is generally considered to be stable in the course of chemical weathering. Nesbitt and Markovics (1997) in their evaluation of the same data set have normalized to Ti because they argue that Al was introduced to some samples by translocation of fine-grained clay minerals into deeper parts of the weathering profile. However, this cannot be solved mathematically because compositional data on their own are in principle not able to decipher what is happening in absolute terms. The only conclusion that can be derived mathematically from the data set is that, relative to Ti, not only Al_2O_3 must have been enriched, but also SiO_2 and K_2O in decreasing proportions (see Fig. 4).

Table 2. Unitary Composition **p** Giving the Direction of the Compositional Linear Trend $L_a(\mathbf{a}; \mathbf{p})$ Adjusted to the Complete Toorongo Data Set (S^{12})

	SiO_2	TiO_2	Al_2O_3	Fe_2O_3	FeO	MnO	MgO	CaO	Na_2O	K_20	P_2O_5	H_2O
$\mathbf{p}_j$	0.0855	0.0818	0.0944	0.1184	0.0581	0.0790	0.0788	0.0494	0.0535	0.0827	0.0780	0.1404

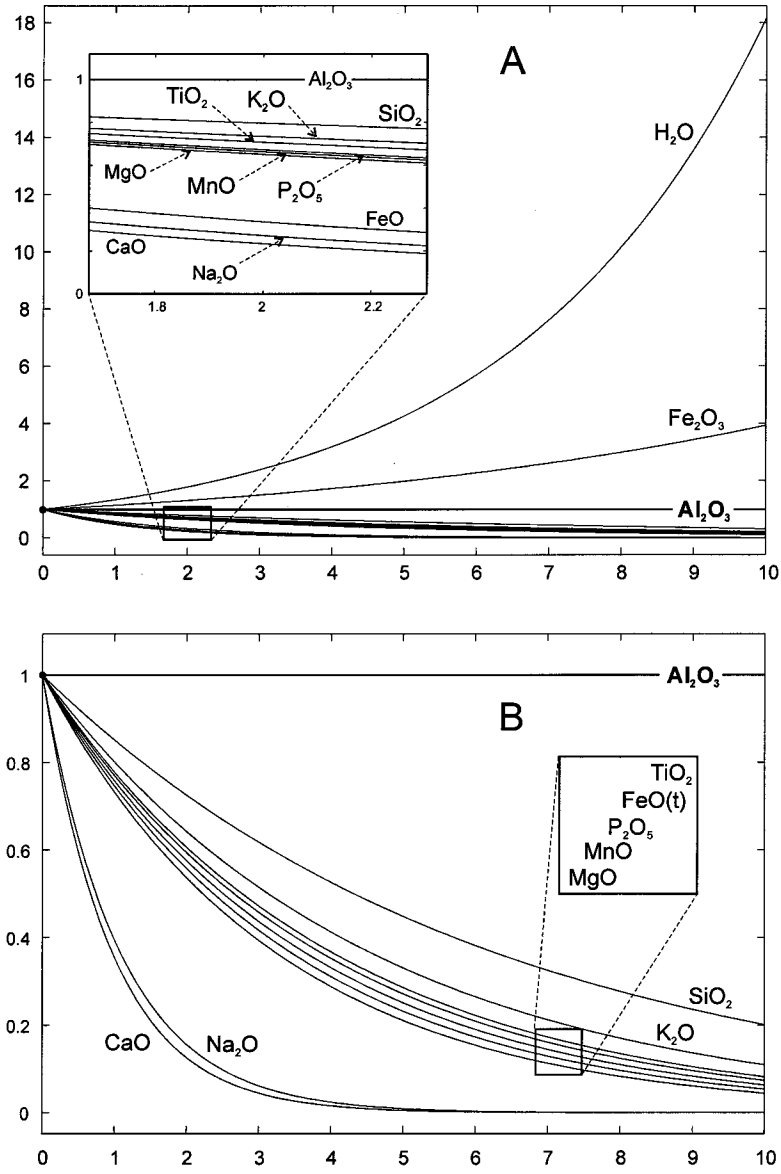

Figure 4. Relative variation diagrams of variables normalised to $Al_2O_3 = 1$ of the compositional linear trend L_a(**a**; **p**) adjusted to the Toorongo data set. (A): Calculations using all variables (S^{12}); (B): calculations using all variables except for H_2O and with total iron FeO(t) (S^{10}). The x-axis is the parameter k of the trend. The y-axis is the relative change of the variable/Al_2O_3 ratio at a given k compared to the initial variable/Al_2O_3 ratio in **a**, e.g., at $k = 2$ CaO/Al_2O_3 and Na_2O/Al_2O_3 ratios are less than 20% of the initial ratios in **a**.

From Table 2 we can observe that only two ratios, $p_{H_2O}/p_{Al_2O_3}$ and $p_{Fe_2O_3}/p_{Al_2O_3}$, will have values greater than 1. This means that only the two variables H_2O and Fe_2O_3 are enriched relative to Al_2O_3. Three of the variables, CaO, Na_2O, and FeO, decrease relatively fast ($p_{CaO}/p_{Al_2O_3}$, $p_{Na_2O}/p_{Al_2O_3}$, $p_{FeO}/p_{Al_2O_3} \approx 0.6$) whereas all the other variables decrease comparatively slowly relative to Al_2O_3. Mineralogically, this observation is consistent with the decomposition of plagioclase (CaO and Na_2O from anorthite and albite components of plagioclase, respectively), the formation of water-rich secondary phyllosilicates (e.g., kaolinite: Al remains stable and H_2O is introduced), and the oxidation of ferrous iron FeO from mafic minerals (here mostly biotite) to ferric iron Fe_2O_3. Figure 4(A) shows the curves of relative change of all variables relative to Al_2O_3.

Because chemical major element analyses of soils and rocks often do not comprise precise data on H_2O content and do not separate between FeO and Fe_2O_3 (e.g., XRF-analyses), it is also worth considering the Toorongo data set excluding H_2O and with total iron FeO(t) instead of taking FeO and Fe_2O_3 separately. In this case, the estimation of the unitary perturbation **p** of the compositional linear trend $L_a(\mathbf{a}; \mathbf{p})$ adjusted to $\mathbf{x}_3, \ldots, \mathbf{x}_{15}$ is given in Table 3. The proportion of the total variability of $\mathbf{x}_3, \ldots, \mathbf{x}_{15}$ with respect to **a** captured by this compositional linear trend is equal to 97.2%.

From Table 3, we can observe that all the ratios $p_j/p_{Al_2O_3}$ will be lower than 1. This means that all variables decrease relative to Al_2O_3 in the course of the weathering process (see Fig. 4(B)). CaO and Na_2O show the strongest decrease; both behave quite similarly as already indicated by their close proximity in the biplots. This has a mineralogical justification, as they are largely derived from the same mineral, i.e., plagioclase. SiO_2 shows the slowest decrease relative to Al_2O_3, and K_2O decreases at still slow, but slightly higher rates. The former is due to only little alteration of quartz (Nesbitt and Markovics, 1997) and in part fixation of silica from weathered feldspars in clay minerals. The latter is due to much lower K-feldspar weathering rates compared to plagioclase and a considerable amount of potassium is still fixed to clay minerals (e.g. illite). A third group of variables, TiO_2, FeO(t), P_2O_5, MnO, and MgO, shows an intermediate behavior in terms of decrease relative to Al_2O_3. Especially the FeO(t)/TiO_2 ratios of the modelled trend are very close to 1 and, thus, show no significant change compared with the original (starting) composition. This observation is mineralogically justified by

Table 3. Unitary Composition **p** Giving the Direction of the Compositional Linear Trend $L_a(\mathbf{a}; \mathbf{p})$ Adjusted to Toorongo Data Set Using All Variables Except for H_2O and With Total Iron FeO(t) Instead of Taking FeO and Fe_2O_3 Separately (S^{10})

	SiO_2	TiO_2	Al_2O_3	FeO(t)	MnO	MgO	CaO	Na_2O	K_20	P_2O_5
$\mathbf{p}_j$	0.1181	0.1093	0.1385	0.1085	0.1040	0.1030	0.0490	0.0554	0.1116	0.1026

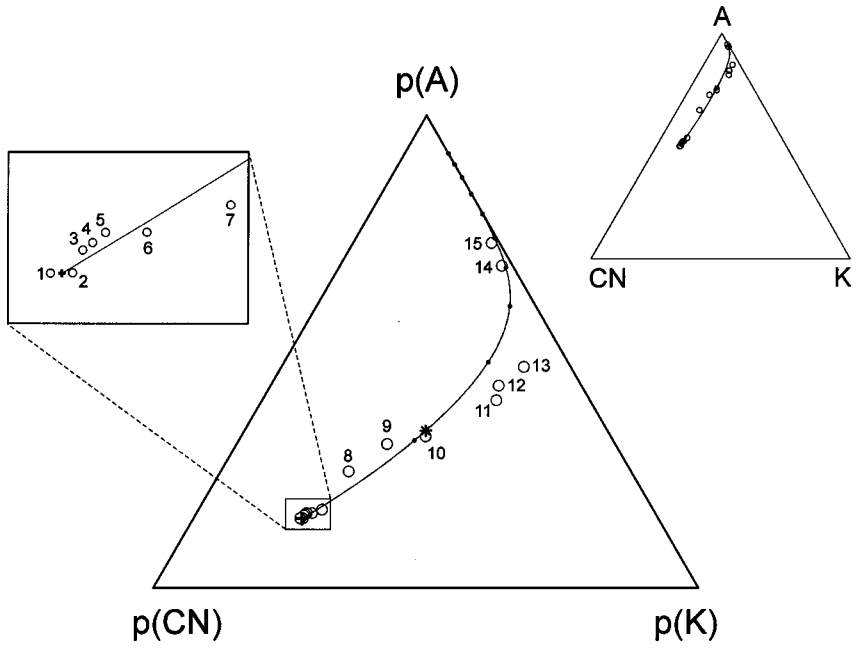

Figure 5. Centred A-CN-K diagram (compare Fig. 1(B)) with the adjusted compositional linear trend $L_a(\mathbf{a}; \mathbf{p})$. Original A-CN-K diagram for comparison. Star indicates the geometric mean of the data set. Bold cross is the starting composition equal to the geometric mean of samples 1 and 2. Filled circles correspond to perturbed compositions $\mathbf{y}_k = \mathbf{a} \oplus (k \otimes \mathbf{p})$, for $k = 1$–10, along the chemical weathering trend.

abundant secondary iron oxides surrounding biotite in weathered samples (Nesbitt and Markovics, 1997).

Reducing the variables to the three-part simplex A-CN-K (compare Fig. 1) allows us to illustrate the compositional linear trend $L_a(\mathbf{a}; \mathbf{p})$ adjusted to $\mathbf{x}_3, \ldots, \mathbf{x}_{15}$ in a ternary diagram (Fig. 5). In this case, the unitary perturbation vector of the trend is given by $\mathbf{p} = [0.4935, 0.1296, 0.3769]$. The proportion of the total variability of $\mathbf{x}_3, \ldots, \mathbf{x}_{15}$ with respect to $\mathbf{a}$ captured by this compositional linear trend is equal to 99.5% and is regarded as a very precise approximation of the chemical weathering trend in the A-CN-K space.

The relative variation diagram (Fig. 6) shows, in addition to the modelled trend for each variable normalized to Al_2O_3, the individual values from each sample used to calculate the weathering trend. To calculate the appropriate k for each composition, we use the orthogonal projection of each composition onto the compositional linear trend. Note that, whereas CN ($CaO^* + Na_2O$) data match very precisely the modelled trend, the K_2O data show considerable scatter around it, especially concerning samples 8, 9, 11, 12, and 13. These samples also lie somewhat

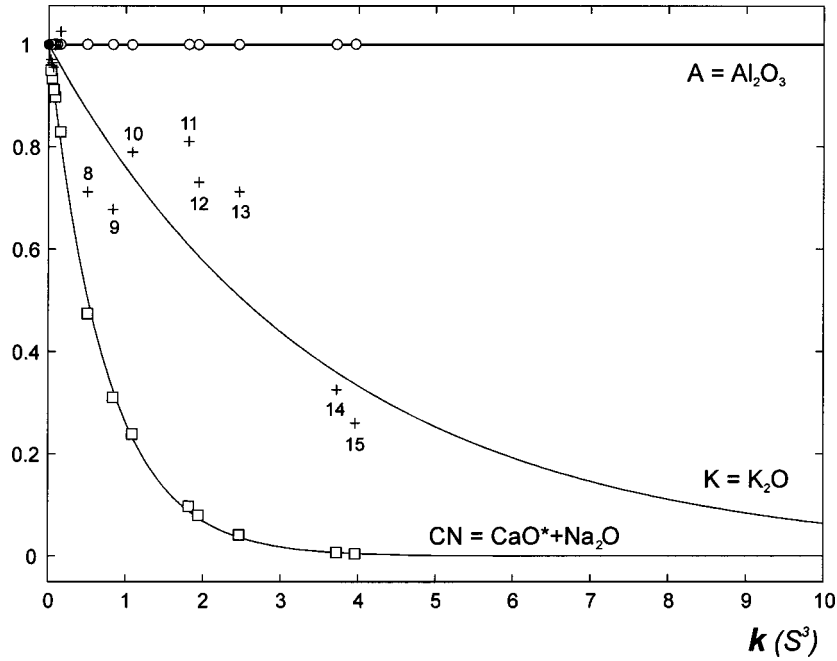

Figure 6. Relative variation diagram (compare Fig. 4) of the compositional linear trend L_a (**a**; **p**) adjusted to the Toorongo data set in the A-CN-K diagram, and, in addition, the data which were used to model the trend. For plotting the data into this diagram, they must be perturbed by the inverse of the starting composition **a**. The parameter *k* ranges from 0.0334 for sample 3 to 3.9393 for sample 15.

off the trend in the ternary diagram (Fig. 5). K_2O/Al_2O_3 ratios appear to show no strict continuous evolution as for example $(CaO^* + Na_2O)/Al_2O_3$ ratios, but reflect discrete groups scattering around the general trend of decreasing K_2O/Al_2O_3 ratios (Fig. 6) This observation suggests that K_2O is possibly not the best candidate for measuring continuously the degree of alteration in, at least, this weathering profile.

DISCUSSION

Based on dissolution kinetics, inferred from experimental work, there is much evidence that weathering of silicate minerals in natural environments is a linear process controlled by surface reactions between minerals and aqueous phases (e.g., Furrer and Stumm, 1986). This linearity is reflected by the statistical results presented here because between 95.9% (all variables, in S^{12}) and 99.5% (A-CN-K, in S^3) of the total compositional variability of the Toorongo weathering profile can be explained by a compositional linear trend.

The Toorongo weathering profile is generally regarded as a good example describing the major processes involved in chemical weathering of the earth's upper crust (e.g., Nesbitt, Markovics, and Price, 1980). If so, the modelled weathering trend should closely resemble compositional data derived from suspended sediment of the world's major rivers and of erosional products of some of the world's major denudation areas (McLennan, 1993). The 23 samples are represented in Figure 7 together with the adjusted compositional linear trend $L_a(\mathbf{a}^*; \mathbf{p}^*)$, where $\mathbf{a}^*$ represents the average upper continental crust (Taylor and McLennan, 1985). Table 4 gives the unitary perturbation vectors within the A-CN-K simplex calculated for both the Toorongo weathering profile and for the data set of McLennan (1993). The close similarity of the two unitary perturbation vectors confirms the

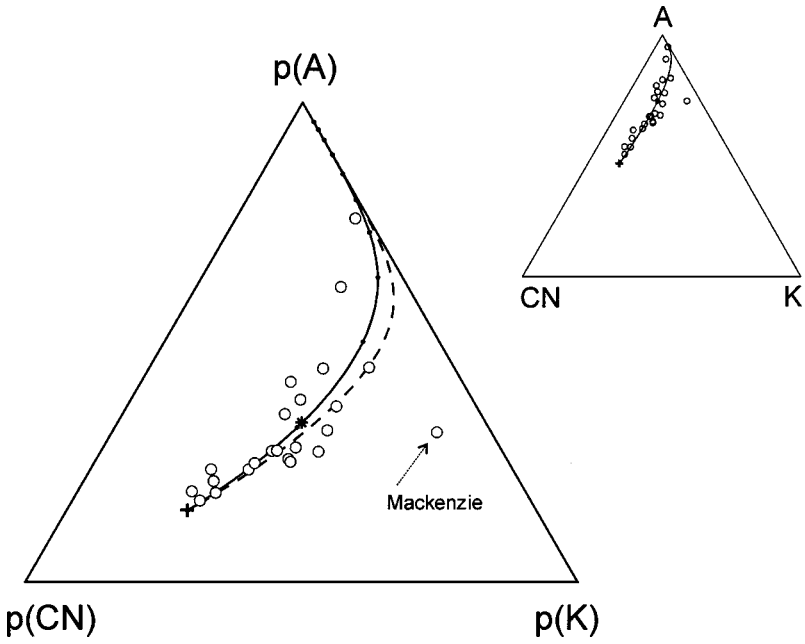

Figure 7. Centred A-CN-K diagram of chemical compositions from suspended sediment of the world's major modern rivers and of recent erosional products derived from the worlds major denudation areas (McLennan, 1993). Sediment from the Mackenzie river, the only arctic river in this study, lies somewhat off the trend. Solid line shows compositional linear trend $L_a(\mathbf{a}^*; \mathbf{p}^*)$ adjusted to the data set using as starting composition $\mathbf{a}^*$ (bold cross) the average upper continental crust (Taylor and McLennan, 1985). This trend captures 97.1% of the total variability. The stippled line represents the compositional linear trend $L_a(\mathbf{a}^*; \mathbf{p})$ where $\mathbf{p}$ is the unitary perturbation vector derived from the A-CN-K Toorongo weathering profile using average upper continental crust as starting composition. Filled circles correspond to perturbed compositions $\mathbf{y}_k = \mathbf{a}^* \oplus (k \otimes \mathbf{p})$ $(k = 1, 2, \ldots, 10)$ along the chemical weathering trend. Star represents the geometric mean of the data set. Original A-CN-K diagram for comparison.

Table 4. Unitary Compositions **p** of the Compositional Linear Trends $L_a(\mathbf{a}; \mathbf{p})$ Adjusted to Different A-CN-K Data Sets and Percentage of Variability Explained the Trends

p_A	p_{CN}	p_K	Starting composition **a**	% Explained variability	Data base (reference)
0.4935	0.1296	0.3769	Geometric mean of samples 1 and 2	99.5	Toorongo weathering profile (Nesbitt and Markovics, 1997)
0.5109	0.1307	0.3583	Average upper continental crust	97.1	Major rivers and denudation areas (McLennan, 1993)

Toorongo weathering profile being a very well suited example to study chemical weathering in general terms. On average, the compositional linear trend describing chemical weathering of the earth's upper crust appears to be well estimated by $L_a(\mathbf{a}^*;[0.51, 0.13, 0.36])$ within the three-part simplex A-CN-K.

The calculation of compositional trends related to specific geological processes has the potential to validate hypotheses on individual sediment compositions with regard to their predepositional and/or diagenetic history. In our example this means that defining a compositional linear trend for chemical weathering allows us to check for a given soil or sediment sample derived from a known source rock composition, if the sample may be directly derived from the source rock by chemical weathering or if another process (e.g., sedimentary sorting, diagenesis, metasomatism) or a combination of processes must be responsible for the observed composition of the sample.

If a sample **s** is exclusively derived from chemical weathering of the source rock **g** described by the linear compositional trend $L_a(\mathbf{g}; \mathbf{p}_w)$ defined by the unitary perturbation vector $\mathbf{p}_w = [0.4935, 0.1296, 0.3769]$, it implies that there exists a scalar k_w which satisfies the condition $\mathbf{s} = \mathbf{g} \oplus (k_w \otimes \mathbf{p}_w)$ within reasonable error. If no such k_w exists, but there is evidence for at least some chemical weathering, we can look for a combination of chemical weathering and other processes which might be capable to explain the observed composition of the sample in question. Thus, if a second process—determined by another unitary perturbation vector $\mathbf{p}_m$—is responsible for the deviation of the sample from the chemical weathering trend, the following equation has to be satisfied by some scalars k_m and k_w:

$$\mathbf{s} = \mathbf{g} \oplus (k_w \otimes \mathbf{p}_w) \oplus (k_m \otimes \mathbf{p}_m) \tag{3}$$

To illustrate this approach, we have chosen an example where chemically altered early Proterozoic paleosoils which were developed on a late Archean granite were later affected by K-metasomatism (Fedo, Nesbitt, and Young, 1995; Rainbird, Nesbitt, and Donaldson, 1990). Consequently, the samples are moved away from the predicted trend of chemical weathering towards higher K_2O contents (Fig. 8).

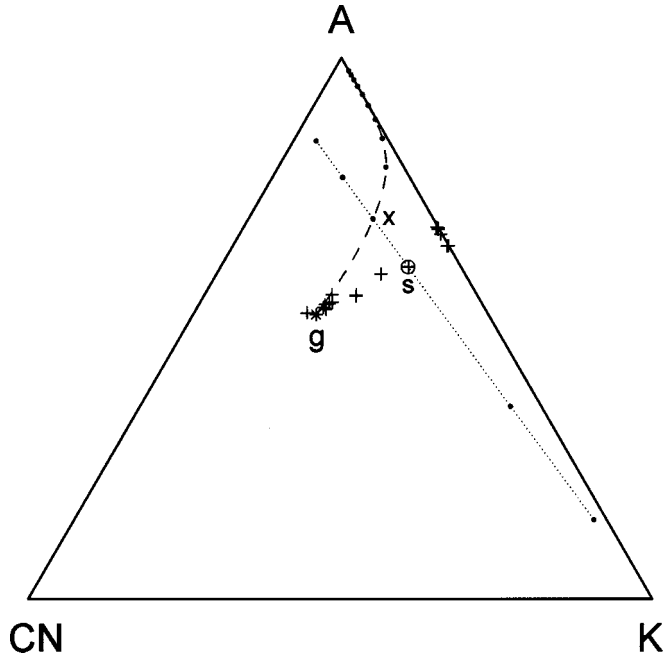

Figure 8. A-CN-K diagram showing composition of samples from an early Proterozoic paleosoil developed on Late Archean granites at Ville Marie in Quebec, Canada (Rainbird, Nesbitt, and Donaldson, 1990). Stippled line shows chemical weathering trend $L_a(\mathbf{g}; \mathbf{p}_w)$ using the perturbation vector $\mathbf{p}_w = [0.4935, 0.1296, 0.3769]$ calculated for the Toorongo weathering profile and the sample **g** with the lowest CIA value as starting composition ($\mathbf{g} = [0.5262, 0.2763, 0.1975]$, $k_w = 1, 2, \ldots, 10$). Dotted line shows the compositional linear trend $L_a(\mathbf{s}; \mathbf{p}_m)$ of K-metasomatism where $\mathbf{p}_m = [0.1851, 0.1851, 0.6299]$ and $\mathbf{s} = [0.6143, 0.0846, 0.3012]$ ($k_m = -2, \ldots, 0, \ldots, 2$). The intersection of both compositional linear trends in $\mathbf{x} = [0.7021, 0.0967, 0.2012]$ corresponds to $k_w = 1.0010$ and $k_m = -0.4385$.

K-metasomatism essentially adds K_2O to the sediments but does not change the ratios between the other variables and, therefore, the effects of K-metasomatism in the A-CN-K simplex can be described by a compositional linear trend through **s**, $L_a(\mathbf{s}; \mathbf{p}_m)$ whose direction is independent of **s** and is given by the unitary perturbation vector $\mathbf{p}_m = [0.1851, 0.1851, 0.6299]$. It is characterized by two identical components. Given a composition **s**, Eq. (3) can be solved leading to unique solutions for both k_w and k_m (Fig. 8). The unique point of intersection of the weathering trend and the metasomatism trend is composition **x**, which is defined by $\mathbf{x} = \mathbf{g} \oplus (k_w \otimes \mathbf{p}_w) = \mathbf{s} \oplus (k_m \otimes \mathbf{p}_m)^{-1}$.

The compositional evolution of an individual sample can now be precisely traced from the original composition of the Ville Marie granite **g** to its present

composition in, e.g., point **s** (Fig. 8). First, the composition of the precursor sediment affected by chemical weathering moved along the chemical weathering trend $L_a(\mathbf{g}; \mathbf{p}_w)$ up to composition **x**, which reflects the state of chemical weathering of the sample before the onset of K-metasomatism. Later, the sediment was affected by K-metasomatism moving its composition along the metasomatism trend $L_a(\mathbf{s}; \mathbf{p}_m)$ from composition **x** to the present-day composition **s** of the sample.

Finally, we would like to discuss some alternatives to CIA as a measure of the degree of chemical weathering. This is motivated by the nonadditive and nontranslation invariant properties of CIA (see above), which is directly related to the relative nature of compositional data. Certainly, an increase of a fixed amount in CIA values does not directly correlate to a fixed amount of weathering, but depends on where we are in the course of the process. For example, an increase from CIA = 50 to CIA = 60 and from CIA = 80 to CIA = 90 obviously does not relate to the same incremental amount of weathering, as there is no linear relationship between amount of weathering and CIA. However, the parameter k, which identifies a composition on a compositional linear trend $L_a(\mathbf{a}; \mathbf{p})$ provides a direct translation invariant measure of the amount of alteration along a chemical weathering trend: an increase in k of, e.g., 0.5 can be related to a certain amount of weathering regardless of where we are in the course of the process. The relation between k and CIA is illustrated in Figure 9. Translation invariance is also preserved if a simpler parameter than k is chosen to describe the degree of chemical weathering which uses some or all of the CIA variables and is strictly linearly correlated to k. Some possibilities are listed in Table 5 and illustrated in Figure 9.

The parameter $\ln(Al_2O_3/g(ACNK))$ involves all CIA variables and correlates almost perfectly to k ($r^2 > 0.99$). The same quasi-perfect linear correlation is observed for parameters $\ln((CaO^* + Na_2O)/Al_2O_3)$ and $\ln(Na_2O/Al_2O_3)$ whereas $\ln(K_2O/Al_2O_3)$ shows a significantly lower correlation coefficient ($r^2 \approx 0.83$). The latter observation is already evident from A-CN-K data (Fig. 6) and suggests that K_2O is a less important variable for describing chemical weathering although using weathering indices without K_2O may give rise to other problems (Fedo, Nesbitt, and Young, 1995). However, if we do not aim at describing the state of weathering of any unknown sample but focus on a specific weathering trend with known source composition, the above-mentioned parameters—$\ln(Al_2O_3/g(ACNK))$, $\ln((CaO^* + Na_2O)/Al_2O_3)$, and $\ln(Na_2O/Al_2O_3)$—allow us to measure precisely the degree of alteration along this trend. Using $\ln(Na_2O/Al_2O_3)$ has the additional advantage of avoiding uncertainties concerning the correction for CaO associated with phosphate and especially carbonate phases (see above).

In general, we have to keep in mind that the assumed compositional linearity of the process can only be achieved if porosity and permeability in the weathering zone are high enough to keep weathering solutions undersaturated with respect to the considered minerals. For example, the reason for the deviation of the K_2O

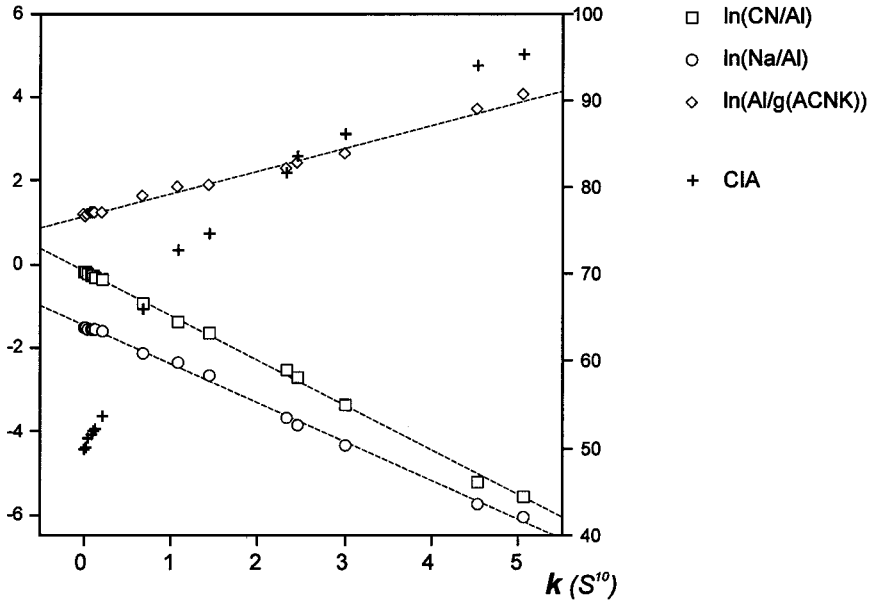

Figure 9. Correlation diagram between the parameter k of the compositional linear trend L_a(**a**; **p**) calculated for the Toorongo weathering profile in S^{10} and three parameters which can be used as translation invariant scales of the weathering trend. For correlation coefficients see Table 5. For comparison, CIA values are plotted (scale on the left side) showing no linear correlation to the parameter k of the compositional linear trend.

data of the Toorongo profile from the modelled trend might be the saturation of weathering solutions for K-feldspar in some levels of the weathering profile. Another reason might be precipitation of K-bearing phases (e.g., illite) leading to selective fixation of potassium and, consequently, a deviation of some samples from the modelled trend towards higher potassium contents.

Table 5. Linear Correlation Coefficients (r^2) Between Parameter k Calculated From the Compositional Linear Trend L_a(**a**; **p**) and Some Other Parameters Using CIA Variables Al_2O_3, CaO^*, Na_2O, and K_2O in S^{10} (see Fig. 4(B))

ln (Na_2O/Al_2O_3)	0.9980
ln (CaO/Al_2O_3)	0.9874
ln (K_2O/Al_2O_3)	0.8303
ln (($CaO^* + Na_2O$)/Al_2O_3)	0.9980
ln (Al_2O_3/g(ACNK))[a]	0.9923

[a] g(ACNK) denotes the geometric mean of the variables CaO, Na_2O, K_2O, Al_2O_3 of each composition.

CONCLUSIONS

(1) Trends in ternary diagrams can be very precisely modelled by a compositional linear trend $L_a(\mathbf{a}; \mathbf{p})$, where **a** represents the initial (or final) composition of the trend and **p** represents the unitary perturbation vector obtained from noncentred principal component analysis by using **a** as the origin. This approach holds for compositional data with any number of parts.

(2) The chemical weathering trends defined—locally—by the Toorongo weathering profile and—at global scales—by sediments derived from the world's major rivers and from some major denudation areas reveal close similarities suggesting that (i) the processes behind both data sets are similar and (ii) the Toorongo profile provides a very good example for studying chemical weathering at outcrop scales. The compositional linear trend describing chemical weathering of the earth's upper crust is well estimated by $L_a(\mathbf{a}^*;[0.51, 0.13, 0.36])$ within the A-CN-K simplex, where $\mathbf{a}^*$ represents the average upper continental crust.

(3) Modelling compositional linear trends provides a useful approach for validating individual processes behind individual trends, and for quantifying the combined effects of different processes, which might have modified the composition of soils, sediments, and rocks.

(4) Alternatively to CIA, we suggest translation invariant measures for the degree of chemical weathering along the compositional linear trend. These are $\ln(Al_2O_3/g(ACNK))$, $\ln((CaO^* + Na_2O)/Al_2O_3)$, and $\ln(Na_2O/Al_2O_3)$, with the latter having the additional advantage of avoiding uncertainties concerning the correction for CaO associated with nonsilicate phases.

ACKNOWLEDGMENTS

This study is financially supported by the German Research Foundation (Grant No. EY 23/2) and by the Dirección General de Investigación of the Spanish Ministry for Education and Culture (project BFM2000-0524). We thank John Aitchison for constructive criticism and helpful discussion.

REFERENCES

Aitchison, J., 1986, The statistical analysis of compositional data: Chapman and Hall, London, 416 p.

Aitchison, J., 1990, Relative variation diagrams for describing patterns of compositional variability: Math. Geol., v. 22, p. 487–511.

Aitchison, J., and Greenacre, M., 2002, Biplots of compositional data: Appl. Stat., v. 51, no. 4, p. 375–392.

Barceló-Vidal, C., Martín-Fernández, J. A., and Pawlowsky-Glahn, V., 2001, Mathematical foundations for compositional data analysis, *in* Proceedings of IAMG'01—The Annual Conference of the International Association for Mathematical Geology, Cancún, México, 20 p. (CD-Rom).

Buxeda i Garrigós, J., 1999, Alteration and contamination of archaeological ceramics: The perturbation problem: J. Archaeol. Sci., v. 26, p. 295–313.

Fedo, C. M., Nesbitt, H. W., and Young, G. M., 1995, Unravelling the effects of potassium metasomatism in sedimentary rocks and paleosoils, with implications for paleoweathering and provenance: Geology, v. 23, p. 921–924.

Furrer, G., and Stumm, W., 1986, The coordination chemistry of weathering, 1. Dissolution kinetics of δ-Al_2O_3 and BeO: Geochim. Cosmochim. Acta, v. 50, p. 1847–1860.

Gabriel, K. R., 1971, The biplot-graphic display of matrices with applications to principal component analysis: Biometrika, v. 58, p. 453–467.

Lebart, L., Morineau, A., and Piron, M., 1995, Statistique exploratoire multidimensionnelle: Dundod, Paris, 439 p.

Leeder, M., 1999, Sedimentology and sedimentary basins: Blackwell Science, Oxford, 592 p.

McLennan, S. M., 1993, Weathering and global denudation: J. Geol., v. 101, p. 295–303.

Nesbitt, H. W., and Markovics, G., 1997, Weathering of granodioritic crust, long-term storage of elements in weathering profiles and petrogenesis of siliciclastic sediments: Geochim. Cosmochim. Acta, v. 61, p. 1653–1670.

Nesbitt, H. W., Markovics, G., and Price, R. C., 1980, Chemical processes affecting alkalis and alkaline earths during continental weathering: Geochim. Cosmochim. Acta, v. 44, p. 1659–1666.

Nesbitt, H. W., and Young, G. M., 1982, Early Proterozoic climates and plate motions inferred from major element chemistry of lutites: Nature, v. 299, p. 715–717.

Nesbitt, H. W., and Young, G. M., 1984, Prediction of some weathering trends of plutonic and volcanic rocks based on thermodynamic and kinetic considerations: Geochim. Cosmochim. Acta, v. 48, p. 1523–1534.

Pawlowsky-Glahn, V., and Egozcue, J. J., 2002, About BLU estimators and compositional data: Math. Geol., v. 34, no. 3, p. 259–274.

Rainbird, R. H., Nesbitt, H. W., and Donaldson, J. A., 1990, Formation and diagenesis of a sub-Huronian saprolith: Comparison with a modern weathering profile: J. Geol., v. 98, p. 801–822.

Schechter, E., 1997, Handbook of analysis and its foundations: Academic Press, San Diego, 883 p.

Taylor, S. R., and McLennan, S. M., 1985, The continental crust: Its composition and evolution: Blackwell Science, Oxford, 315 p.

von Eynatten, H., Barceló-Vidal, C., and Pawlowsky-Glahn, V., 2003, Sandstone composition and discrimination: A statistical evaluation of different analytical methods: J. Sediment. Res., v. 73, no. 1, p. 47–57.

von Eynatten, H., Pawlowsky-Glahn, V., and Egozcue, J. J., 2002, Understanding perturbation on the simplex: A simple method to better visualise and interpret compositional data in ternary diagrams: Math. Geol., v. 34, no. 3, p. 249–257.